nature immunology

Immune complex relay by subcapsular sinus macrophages and noncognate B cells drives antibody affinity maturation

Tri Giang Phan[1,2], Jesse A Green[1,3], Elizabeth E Gray[1,3], Ying Xu[1] & Jason G Cyster[1]

Subcapsular sinus (SCS) macrophages capture antigens from lymph and present them intact for B cell encounter and follicular delivery. However, the properties of SCS macrophages are poorly defined. Here we show SCS macrophage development depended on lymphotoxin-α1β2, and the cells had low lysosomal enzyme expression and retained opsonized antigens on their surface. Intravital imaging revealed immune complexes moving along macrophage processes into the follicle. Moreover, noncognate B cells relayed antigen opsonized by newly produced antibodies from the subcapsular region to the germinal center, and affinity maturation was impaired when this transport process was disrupted. Thus, we characterize SCS macrophages as specialized antigen-presenting cells functioning at the apex of an antigen transport chain that promotes humoral immunity.

Early studies tracking the fate of opsonized antigens arriving in lymph nodes showed that large amounts of antigen were trapped and catabolized by macrophages in the medulla, whereas smaller amounts were captured by macrophages lining the subcapsular sinus (SCS)[1–3]. SCS macrophages efficiently capture several types of particulate antigen and facilitate their display for cognate recognition by follicular B cells[4–6]. In one study it was shown that immune complexes could be captured from SCS macrophages by noncognate B cells through complement receptors 1 and 2 (CR1/2; A000541), and these cells mediated immune complex delivery to follicular dendritic cells (FDCs) in primary follicles[5]. SCS macrophages thus have an established role as antigen-presenting cells for B cells. However, in contrast with the wealth of information available regarding dendritic cells, the antigen-presenting cells of the T zone[7], SCS macrophages have not been isolated in pure form and little is known about their cell biological properties or developmental requirements.

In a primary immune response, initial antibody secretion occurs within 3–5 d and the germinal center (GC) response peaks several days later[8]. The GC is characterized as a site where newly mutated B cells compete for antigen, allowing selection events to occur that lead to antibody affinity maturation[9]. Immune complexes are displayed within GCs, particularly on light zone FDCs, but GCs have generally been thought to exclude follicular B cells, and the mechanism of immune complex delivery to GCs has not been established. However, recent real-time imaging studies have provided evidence that follicular B cells can indeed access the GC light zone[10,11], raising the possibility that immune complex relay is involved in delivery of antigen and newly formed antibody to GCs.

Here we have used surface phenotyping of isolated cells to distinguish SCS macrophages from two populations of medullary macrophages. SCS macrophages were smaller and had lower expression of lysosomal enzymes. SCS macrophages displayed immune complexes on their surface and delivered complexes unidirectionally along processes that extended into the follicle. These cells were dependent on the cytokine lymphotoxin, derived from B cells, for their development and function. Disruption of the immune complex relay from SCS macrophages to FDCs by removing CR1/2 from noncognate B cells led to a reduction in antibody affinity maturation, establishing a role for immune complex relay in driving the GC response.

RESULTS

Isolation and identification of SCS macrophages

On the basis of *in situ* staining, both SCS and medullary macrophages express the sialic acid–binding, immunoglobulin-like, C-type lectin sialoadhesin (CD169) recognized by the monoclonal antibodies (mAbs) Ser-4 and MOMA-1 (ref. 12 and **Fig. 1a**). However, $CD169^+$ macrophages lining the SCS can be distinguished from those lining the medullary sinuses in lymph node sections by their lack of staining with the F4/80 mAb (ref. 13 and **Fig. 1a**). To isolate and identify SCS macrophages, we digested lymph nodes with a protease cocktail and stained single-cell suspensions with mAbs to CD11b (CR3, also called Mac1), CD11c (CR4), CD169 and F4/80 antigen for flow cytometry. This analysis revealed distinct populations of $CD11b^+CD11c^{lo}$ macrophages and $CD11b^+CD11c^{hi}$ classical dendritic cells (**Fig. 1b**). We excluded $CD11c^{hi}$ cells from our analysis, as macrophages lining the SCS and medullary sinuses have low to undetectable staining for this

[1]Howard Hughes Medical Institute and Department of Microbiology and Immunology, University of California San Francisco (UCSF), California, USA. [2]Garvan Institute of Medical Research, Darlinghurst, Sydney, New South Wales, Australia. [3]These authors contributed equally to this work. Correspondence should be addressed to T.G.P. (t.phan@garvan.org.au) or J.G.C. (jason.cyster@ucsf.edu).

Received 13 March; accepted 23 April; published online 7 June 2009; doi:10.1038/ni.1745

marker by immunofluorescence microscopy, in contrast to the bright staining of classical dendritic cells residing in the T zone (**Supplementary Fig. 1** online). Further analysis of total CD11b^{+}CD11c^{lo} macrophages for expression of CD169 and F4/80 antigen revealed the CD169^{hi} cells could be divided into F4/80-negative and F4/80-positive subsets, as well as a third macrophage population that was CD169^{-}F4/80^{+} (**Fig. 1b**). Immunofluorescence analysis of lymph node sections showed that both CD169^{hi}F4/80^{+} and CD169^{-}F4/80^{+} populations resided in lymph node medullary regions (**Fig. 1a**). Using an alternative gating scheme, it was possible to identify the SCS-lining macrophages as CD169^{hi}CD11c^{lo} cells that expressed CD11b and were negative for F4/80 antigen (**Fig. 1c**). In subsequent experiments we used the CD169^{hi}CD11c^{lo} gating strategy and thus focused our attention on a comparison of the CD169^{hi}F4/80^{-} and the CD169^{hi}F4/80^{+} macrophage subsets. Light-scatter analysis showed that cells in the F4/80^{-} subset were smaller and less granular than those in the F4/80^{+} subset (**Fig. 1d**). We next asked whether these cells were able to capture *in vivo*–generated immune complexes containing the fluorescent dye phycoerythrin (PE)[5]. Both CD169^{hi} macrophage subsets became heavily labeled with PE immune complexes 2 h after PE injection in mice passively immunized with rabbit PE-specific IgG, with the F4/80^{+} medullary cells showing substantially higher labeling (**Fig. 1e**,**f**), and *in vitro* mixing experiments confirmed that the PE immune complex capture occurred *in vivo* rather than during cell isolation (**Fig. 1e**). In contrast, there was no PE immune complex labeling of CD169^{-}F4/80^{+} cells (data not shown). Thus, we could isolate and identify immune complex-capturing SCS macrophages as CD169^{hi}CD11c^{lo}CD11b^{+}F4/80^{-} cells.

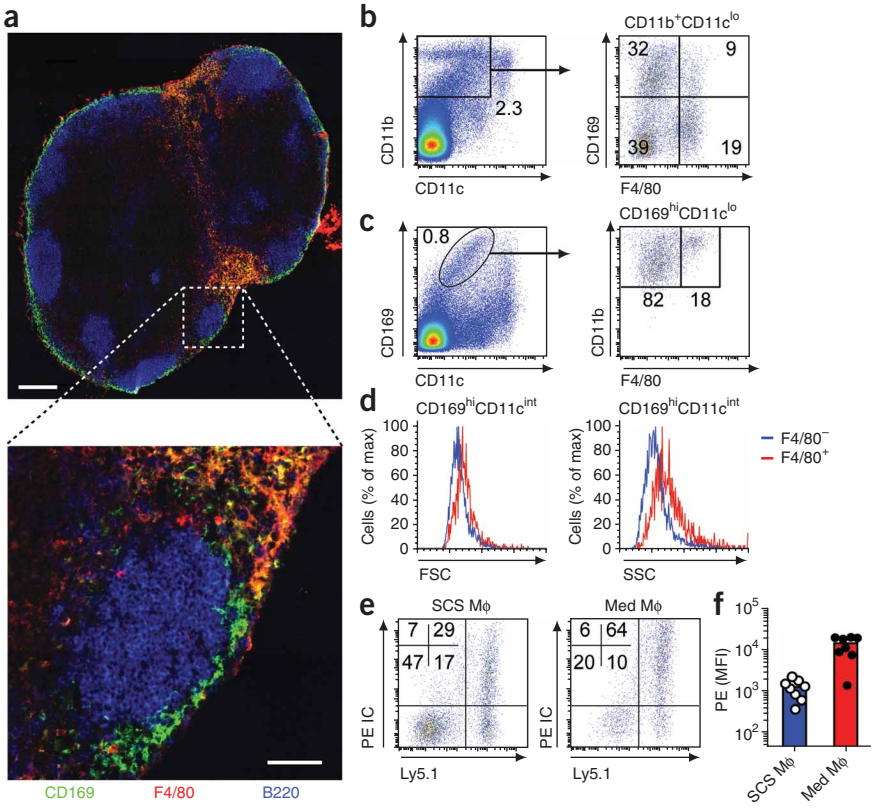

Figure 1 Isolation and identification of SCS macrophages. (**a**) Mosaic fluorescence microscopy of inguinal lymph node stained with mAbs to CD169, F4/80 and B220 to identify SCS and medullary macrophages *in situ*. Scale bars, 200 μm (top); 50 μm in inset (bottom). Representative of three experiments. (**b**,**c**) Pseudocolor plots from flow cytometry of a single-cell suspension of protease-digested peripheral lymph nodes stained with mAbs to CD11b, CD11c, CD169 and F4/80. (**b**) CD11c^{hi} classical dendritic cells can be distinguished from CD11b^{+}CD11c^{lo} macrophages, which can be further resolved into four subpopulations based on CD169 and F4/80. (**c**) Alternative gating strategy showing that CD169^{hi}CD11c^{lo} cells comprise CD11b^{+} cells that are either F4/80^{-} SCS macrophages or F4/80^{+} medullary macrophages. (**d**) Forward-scatter (FSC) and side-scatter (SSC) profiles of SCS and medullary macrophages gated as in **c**. Data in **b**–**d** are representative of >5 experiments. (**e**,**f**) PE immune complex (IC) capture by SCS and medullary (Med) macrophages (Mϕ) 2 h after PE injection. (**e**) Representative pseudocolor plots from three experiments of PE IC capture by CD169^{hi}CD11c^{int}F4/80^{-} SCS and CD169^{hi}CD11c^{int}F4/80^{+} medullary macrophages. Ly5.2^{+} cells serve as *ex vivo* mixing controls. Numbers indicate the percentage of cells in each quadrant. (**f**) Graph of pooled data from three experiments, $n = 5$ mice, showing PE mean fluorescence intensity (MFI) of medullary macrophages and SCS macrophages 2 h after PE injection.

SCS macrophages are poorly endocytic and degradative

To investigate the handling of captured immune complexes by SCS and medullary macrophages, we removed lymph nodes 4 h after PE injection and stripped surface-bound molecules with acetic acid. Notably, acid stripping removed almost all the PE immune complexes from the surface of the SCS macrophages without severely affecting the labeling of the medullary population (**Fig. 2a**,**b**). As another approach to test for PE immune complex internalization, we stained draining lymph node macrophages with antibody against rabbit IgG to detect the passively transferred PE-specific antibody (**Fig. 2c**). This analysis showed that SCS macrophages had lower amounts of PE immune complexes that were protected from anti–rabbit IgG surface staining and therefore presumably located intracellularly (**Fig. 2c**,**d**). To determine the fate of internalized immune complexes, we modified the above protocol and treated mice with an antigen that increases in fluorescence after degradation. Mice were given Alexa Fluor 647–labeled bovine serum albumin (BSA)-specific polyclonal rabbit IgG and then subcutaneously injected with self-quenching DQ Green–BSA extensively haptenated with BODIPY FL fluorophore to generate BSA–anti-BSA immune complexes. After internalization and degradation in lysosomes, the DQ Green–BSA is hydrolyzed to single dye-labeled peptides that fluoresce in the green channel. Such fluorescence was readily observed in medullary but not SCS macrophage populations (**Fig. 2e**). To account for the differential capture of immune complexes, we compared the production of green fluorescence among SCS and medullary macrophages having low, intermediate and high labeling with BSA-specific Alexa Fluor 647–labeled rabbit IgG (**Fig. 2e**). This analysis showed that for the same amount of immune complex capture, medullary macrophages consistently degraded more BSA than SCS macrophages. Taken together these findings suggest that SCS macrophages are a poorly endocytic macrophage population with low degradative capacity that retains immune complexes on the cell surface, whereas

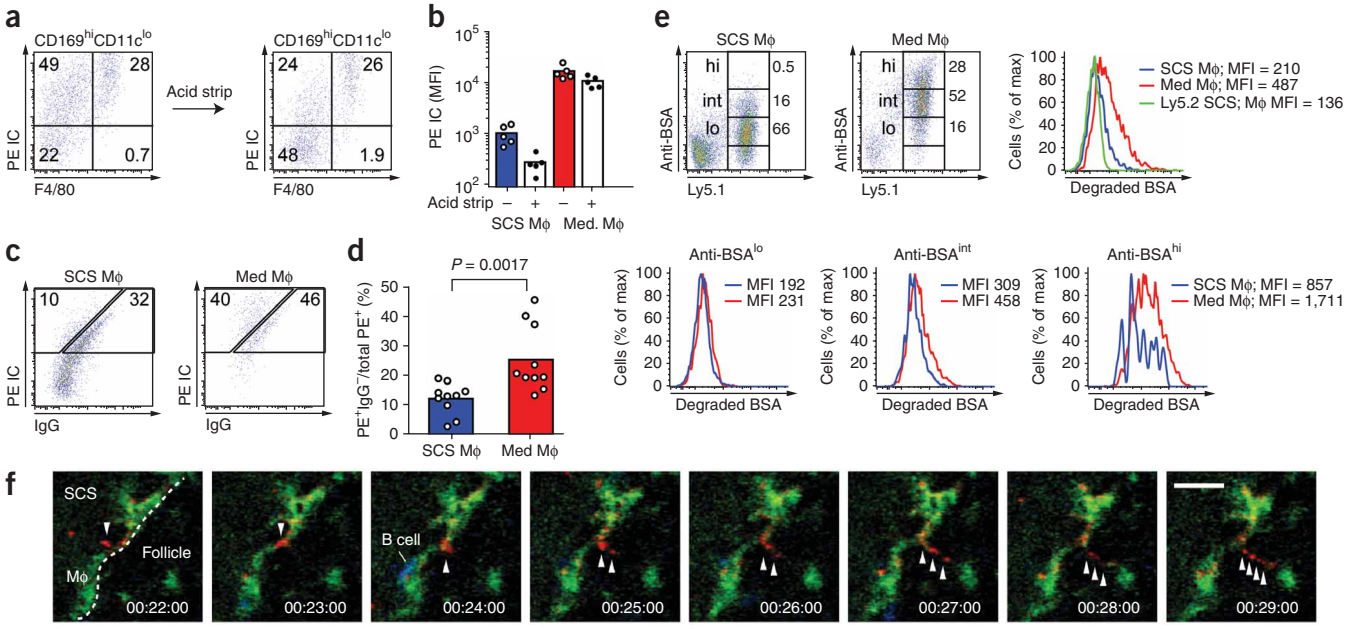

Figure 2 SCS macrophages are poorly endocytic and poorly degradative. (**a**,**b**) Effect of acid stripping on macrophage retention of immune complexes (ICs). (**a**) Representative pseudocolor plots from three flow cytometric experiments on CD169^{hi}CD11c^{lo} cells before and after acid stripping. PE and PE-specific rabbit IgG was injected to generate PE ICs *in vivo* and macrophages (Mϕ) isolated from draining lymph nodes 4 h later. (**b**) Graph showing a pool of mean fluorescence intensity (MFI) data for F4/80^{-} (SCS) and F4/80^{+} (medullary (Med)) cells. Circles, individual lymph nodes; bars, mean (three experiments, $n = 3$ mice). (**c**,**d**) Measurement of IC internalization. (**c**) Cells prepared as in **a** were surface-stained with anti–rabbit IgG to detect PE^{+}IgG^{-} cells. Representative pseudocolor plot from six experiments showing detection of PE IC and rabbit IgG on CD169^{hi}CD11c^{lo}F4/80^{-} SCS and CD169^{hi}CD11c^{lo}F4/80^{+} medullary macrophages. Numbers in **a**,**c** indicate percentage of cells in each gate. (**d**) Graph of percentage of PE^{+}IgG^{-} cells; pooled data from six experiments, $n = 6$ mice. (**e**) Representative pseudocolor plots from three experiments showing gating for SCS and medullary macrophages with low (lo), intermediate (int) and high (hi) amounts of *in vivo*–generated BSA–anti-BSA ICs 4 h after DQ Green–BSA injection. Ly5.2^{+} cells serve as a negative control. Overlay histogram shows amount of BSA degradation by SCS and medullary macrophages with the same abundance of BSA–anti-BSA ICs. (**f**) Time-lapse images from intravital two-photon microscopy (first movie in **Supplementary Movie 1**) showing capture, disaggregation and unidirectional transport of discrete, bright red PE ICs along the cellular process of a SCS macrophage labeled green with CD169-specific mAb. Time stamp is in hh:mm:ss. Scale bar, 10 μm.

medullary macrophages capture larger amounts of immune complexes and are highly endocytic.

SCS macrophages translocate immune complexes

We then performed intravital two-photon microscopy to image the handling of immune complexes by SCS macrophages *in vivo*. To label sinus-lining macrophages, we subcutaneously injected Alexa Fluor 488–conjugated CD169-specific mAb the day before imaging. B cells expressing the reporter cyan fluorescent protein (CFP) were adoptively transferred to delineate lymphoid follicles. Lymph in the SCS in these experiments was clearly visible as granular autofluorescent green material flowing in the space between the blue signal from the second harmonic of collagen in the capsule and the green layer of labeled macrophages lining the floor of the SCS (**Supplementary Movie 1** online). After injection of PE into mice passively immunized with PE-specific rabbit polyclonal antibodies, we observed rapid drainage of PE immune complexes into the SCS, where they were captured and disaggregated before being conveyed along macrophage cell processes from the lumen into the follicle (**Supplementary Movie 1** and **Fig. 2f**). Rare CFP^{+} B cells could be observed moving within the follicle as expected, and, in one instance, a B cell was seen migrating briefly on the sinus-facing side of a macrophage. Analysis of high-resolution images (0.6 μm per pixel) from multiple individual 'confocal' *z* stacks showed that the discrete PE immune complexes appeared to move along the surface membrane of SCS macrophages defined by CD169 labeling. Furthermore, on the occasions where individual cell bodies were clearly defined, the PE immune complexes were rarely observed to be internalized or to travel within the body of the cell. Thus SCS macrophages capture immune complexes and appear to retain them on their surface for rapid translocation into the follicle along cellular processes.

SCS macrophages have low levels of lysosomal enzymes

To investigate the poorly endocytic, poorly degradative nature of SCS macrophages, we asked whether they differentially expressed genes associated with lysosomal degradation. We enriched cells ~5–10-fold from protease-digested peripheral lymph nodes of wild-type mice by Percoll density gradient separation and then sorted them by flow cytometry into DAPI^{-}B220^{-}CD4^{-}CD8^{-}CD169^{hi}CD11c^{lo}CD11b^{+}F4/80^{-}SCS and DAPI^{-}B220^{-}CD4^{-}CD8^{-}CD169^{hi}CD11c^{lo}CD11b^{+}F4/80^{+} medullary macrophages with ~95% purity (**Fig. 3a**). By gene expression analysis, sorted SCS and medullary macrophages showed abundant and similar expression of housekeeping genes (**Fig. 3b**) and a large array of macrophage transcription factors (**Fig. 3c**), confirming that both cell types are of the macrophage lineage. Quantitative (Q)-PCR analysis confirmed that *Sfpi1* transcripts, which encode the macrophage- and B cell–specific transcription factor PU.1, were abundant (**Fig. 3d**). However, SCS macrophages had low abundance of transcripts for lysosome-associated membrane protein (LAMP)-1 and LAMP-2, lysozyme, a panel of lysosomal proteases, and vacuolar ATPases required to acidify the lysosome (**Fig. 3e**). Immunofluorescence microscopy of the isolated cells showed the SCS macrophages were smaller and had markedly reduced LAMP-1 staining compared to medullary macrophages (**Fig. 3f**). Intracellular flow cytometry analysis revealed approximately one-fifth the abundance of LAMP

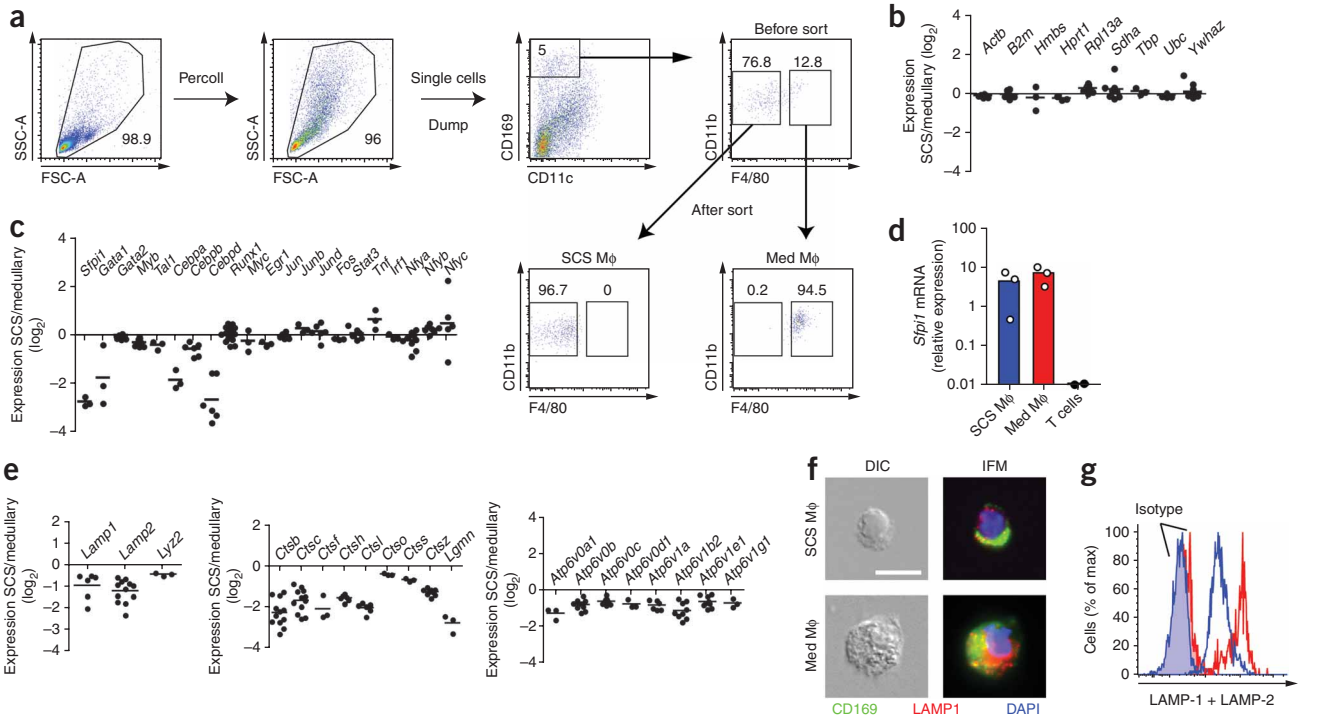

Figure 3 SCS macrophages express low amounts of lysosomal enzymes. (**a**) Single-cell suspensions of protease-digested peripheral lymph nodes were enriched for large, low-density cells by Percoll density gradient. Single DAPI$^-$ (live) cells were gated and B220$^+$, CD4$^+$ and CD8$^+$ cells dumped. CD169^{hi}CD11c^{lo}CD11b$^+$F4/80$^-$ cells were sorted as SCS and CD169^{hi}CD11c^{lo}CD11b$^+$F4/80$^+$ cells as medullary (Med) macrophages (Mϕ). Numbers indicate percentage of cells in the gates shown. Pseudocolor plots are representative of three experiments, $n = 10$–15 mice for each sort. FSC-A, forward scatter area; SSC-A, side scatter area. (**b**–**e**) Comparison of the gene expression profiles of purified SCS and medullary macrophages showing housekeeping genes (**b**), macrophage transcription factors (**c**), lysosomal proteins (**e**, left), proteases (**e**, center) and vacuolar ATPases (**e**, right). Each data point represents an independent experiment (three Affymetrix microarray experiments in total). In some cases there were multiple probe-sets for individual genes, and hence more than three data points. (**d**) Q-PCR analysis showing expression of *Sfpi1* (PU.1) relative to housekeeping gene *Hprt1* by purified SCS and medullary macrophages. T cells serve as negative controls. Each data point represents one experiment. (**f**) Microscopy of purified SCS and medullary macrophages showing cell size and granularity by differential interference contrast microscopy (DIC) and immunofluorescence microscopy (IFM) to detect CD169, LAMP-1 and the nucleus (DAPI). (**g**) Intracellular flow cytometry for LAMP-1 and LAMP-2 protein in SCS macrophages (blue) and medullary macrophages (red) compared to isotype control staining. Data in **f**,**g** are representative of three experiments.

protein expression in the SCS macrophages (**Fig. 3g**). These data suggest that SCS macrophages are poorly degradative because of low expression of lysosomal proteins.

SCS macrophages require B cell–derived lymphotoxin

The distribution of SCS macrophages was closely coordinated with the distribution of B cells (**Fig. 1a**), suggesting a morphogenic interplay. Examination of B cell–deficient mice revealed one-tenth the number of SCS macrophages in their inguinal lymph nodes than that in wild-type controls (**Fig. 4a–c**). The macrophages remaining were enriched for cells with an F4/80$^+$ medullary phenotype (**Fig. 4a**,**b**). B cells are a known source of lymphotoxin (LT)-$\alpha_1\beta_2$, a heterotrimeric cytokine that influences macrophage populations in the spleen[14,15]. Whereas transfers of wild-type B cells to B cell–deficient mice could partially restore the SCS macrophage compartment, LTα-deficient B cells were unable to increase the numbers of these cells (**Fig. 4c**). Transgenic overexpression of LT$\alpha_1\beta_2$ selectively in B cells[16] led to a 2–3-fold increase in total SCS macrophage numbers without affecting B cell numbers (**Fig. 4d**) and a thicker layer of SCS macrophages overlying the B cell areas (**Fig. 4e**). SCS and medullary macrophages both expressed transcripts for the lymphotoxin receptor LTβR (**Fig. 4f**) and showed LTβR surface staining by flow cytometry (**Fig. 4g**). In mixed chimeras reconstituted with *Ltbr*$^{-/-}$ (LTβR-deficient) and wild-type bone marrow after irradiation, there was a selective deficiency in *Ltbr*$^{-/-}$ SCS macrophages, establishing an intrinsic requirement for the receptor in these cells or their precursors (**Fig. 4h**). The requirement for LTβR signaling appeared constitutive, as LTβR-Fc treatment for 4 weeks led to an almost complete ablation of this cell population while having a milder effect on medullary macrophage numbers (**Fig. 4i**,**j**). This SCS macrophage ablation in turn led to a severe defect in the ability of follicular B cells to capture PE immune complexes, assessed by examining PE mean fluorescence intensity of draining lymph node B cells isolated 2 h after PE injection (**Fig. 4k**). The PE mean fluorescence intensity of Ly5.2$^+$ B cells added at the time of lymph node cell isolation provides a measure of the 'nonspecific' *in vitro* capture of PE immune complexes (**Fig. 4k**). Furthermore, short-term LTβR blockade for 3 d had little effect on total SCS macrophage cell numbers but did affect their function in PE immune complex capture (**Fig. 4l**, left panel) and caused a reduction in delivery of PE immune complex to follicular B cells (**Fig. 4l**, right panel). Thus, constitutive lymphotoxin signals provided by B cells are important for SCS macrophage development and their efficient relay of immune complexes to follicular B cells.

Noncognate B cells relay immune complexes into the GC

Antigen capture and follicular relay by SCS macrophages is likely to be most active when preformed IgG antibody is available. This notion led us to ask whether the relay of immune complexes by this pathway was

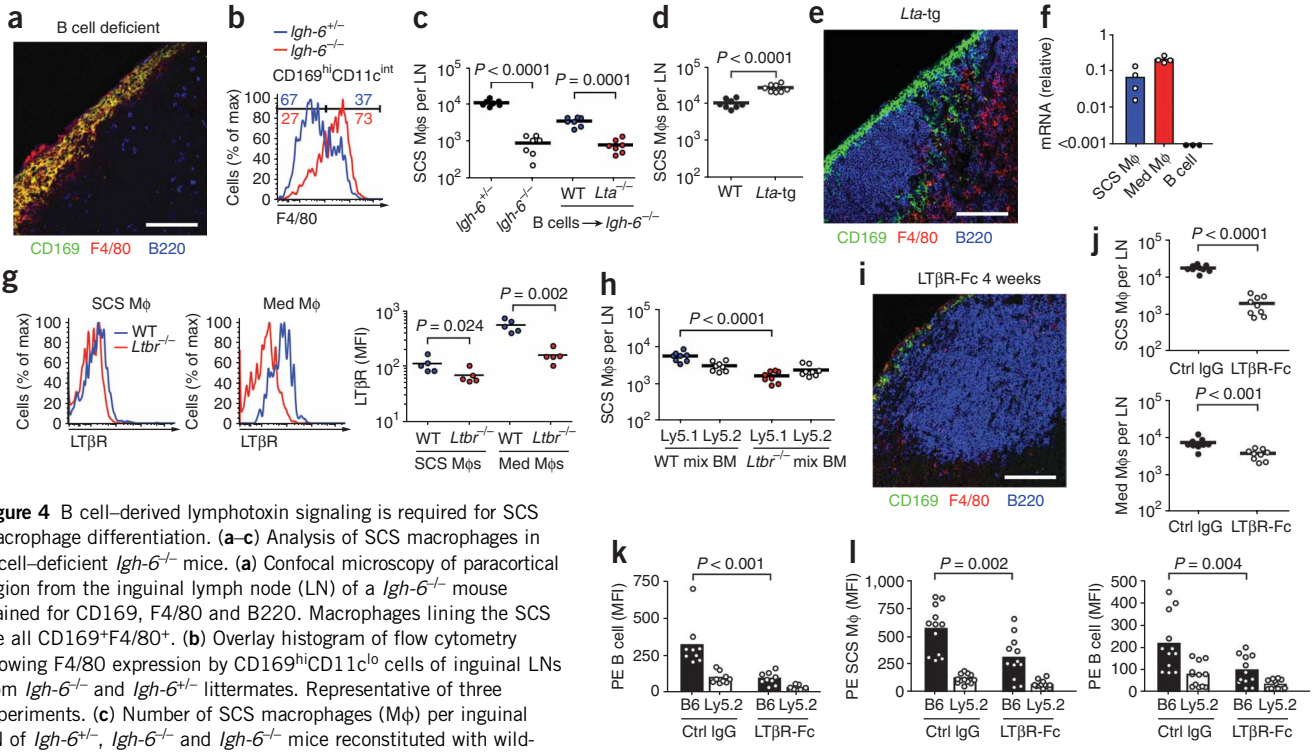

Figure 4 B cell–derived lymphotoxin signaling is required for SCS macrophage differentiation. (**a**–**c**) Analysis of SCS macrophages in B cell–deficient *Igh-6*$^{-/-}$ mice. (**a**) Confocal microscopy of paracortical region from the inguinal lymph node (LN) of a *Igh-6*$^{-/-}$ mouse stained for CD169, F4/80 and B220. Macrophages lining the SCS are all CD169^{+}F4/80^{+}. (**b**) Overlay histogram of flow cytometry showing F4/80 expression by CD169^{hi}CD11c^{lo} cells of inguinal LNs from *Igh-6*$^{-/-}$ and *Igh-6*$^{+/-}$ littermates. Representative of three experiments. (**c**) Number of SCS macrophages (Mϕ) per inguinal LN of *Igh-6*$^{+/-}$, *Igh-6*$^{-/-}$ and *Igh-6*$^{-/-}$ mice reconstituted with wild-type (WT) or *Lta*$^{-/-}$ B cells. (**d**) Number of SCS macrophages per inguinal LN of WT and *Lta*-transgenic (*Lta*-tg) mice. Circles in **c**,**d**, individual inguinal LNs (three experiments, $n = 5$ mice). (**e**) Confocal microscopy, as in **a**, of inguinal LN from *Lta*-tg mouse. Representative of three experiments. (**f**) Q-PCR analysis of LTβR gene expression in purified SCS and medullary (Med) macrophages. Each data point represents one experiment, $n = 10$–15 mice. B cells serve as negative control. (**g**) Left, overlay histograms from flow cytometry for surface expression of LTβR by WT and *Ltbr*$^{-/-}$ SCS and medullary macrophages. Right, graph of LTβR mean fluorescence intensity (MFI). Data are pooled from three experiments, $n = 5$ mice. (**h**) Number of SCS macrophages in WT (blue) and *Ltbr*$^{-/-}$ (red) mixed bone marrow (BM) chimeras. White, Ly5.2 congenic control; circles, individual inguinal LNs (three experiments, $n = 5$ mice). (**i**,**j**) Mice were treated with LTβR-Fc or control human IgG for 4 weeks and LNs stained to detect SCS and medullary macrophages *in situ* (**i**) or by flow cytometry (**j**). (**j**) Number of SCS (left) and medullary (right) macrophages. Circles, individual inguinal LNs (three experiments, $n = 6$ mice); ctrl, control. (**k**) Flow cytometry of PE immune complex capture by follicular B cells 2 h after PE injection in mice treated for 2 weeks with control IgG or LTβR-Fc. Circles, individual inguinal LNs (three experiments, $n = 8$ mice). (**l**) Reduced SCS macrophage and B cell immune complex capture after 3-d LTβR-Fc treatment. Circles, individual LNs (three experiments, $n = 8$ mice). Scale bars, 100 μm.

important during the GC response. To show that newly generated antibodies can feed back to opsonize antigen and form immune complexes for delivery into GCs, we adoptively transferred avian lysozyme–specific Hy10 B cells and ovalbumin (OVA)-specific OT-II T cells and immunized recipient mice with duck egg lysozyme (DEL) conjugated to OVA to provide linked T cell help[11]. Hy10 B cells recognize DEL with low affinity and hen egg lysozyme (HEL) with high affinity. Seven days after primary challenge with DEL-OVA, we rechallenged recipient mice with additional cognate antigen HEL-PE or noncognate nitrophenol-PE as a control. Eight hours after rechallenge we observed deposition of antigen-specific immune complexes containing HEL-PE but not nitrophenol-PE in GCs (**Fig. 5a**). In reciprocal experiments, we transferred 'quasi-monoclonal' QM B cells specific for the hapten nitrophenol (ref. 17) and immunized recipient mice with nitrophenol-conjugated chicken gamma globulin (CGG) (**Fig. 5b**). On day 7 we rechallenged recipient mice with HEL-PE or nitrophenol-PE and observed deposition of nitrophenol-PE–containing immune complexes but not HEL-PE immune complexes. These results indicate that newly generated antibodies opsonize incoming antigen for delivery to GCs and deposition on FDCs.

We next asked whether we could directly visualize transport of opsonized antigen into the GC by noncognate B cells. For tracking studies of cells by real-time, two photon microscopy, only a few percent of the total cells can be labeled[18]. Hy10 B cells expressing green fluorescent protein (GFP) and OT-II T cells were adoptively transferred into either wild-type or *Cr2*$^{-/-}$ bone marrow chimeras (the latter of which lack CR1 and CR2 on endogenous hematopoietic cells but retain these molecules on radiation-resistant FDCs) and the mice were immunized with DEL-OVA to promote lysozyme-specific antibody production and initiate GC formation. We then transferred wild-type polyclonal CFP-transgenic B cells into the mice on day 6. On day 7 HEL-PE was injected subcutaneously to generate red fluorescent antigen–containing immune complexes, and explanted lymph nodes were imaged 3 h later (**Supplementary Movies 2–4** online). At this time point, all detectable GFP^{+} cells correspond to GC B cells[11]. *Cr2*$^{-/-}$ bone marrow chimeras were used as recipients in some experiments in an effort to improve the chances that imaged CFP-transgenic B cells would be immune complex bearing, though similar findings were obtained in *Cr2*$^{-/-}$ (**Supplementary Movies 2** and **4**) and wild-type (**Supplementary Movie 3**) recipients. These two-photon microscopy experiments showed CFP^{+} noncognate B cells loaded with HEL-PE in their trailing uropod migrating from the subcapsular region through the follicular mantle zone into the GFP^{+} GC light zone (**Supplementary Movies 2** and **3** and **Fig. 5c**). CFP^{+} B cells laden with HEL-PE could also be observed migrating deep within the GC light zone (**Supplementary Movie 4**). This antigen transport into GCs was CR1/2-dependent, as delivery of opsonized antigen into GCs was impaired in *Cr2*$^{-/-}$ chimeras that did not contain wild-type polyclonal

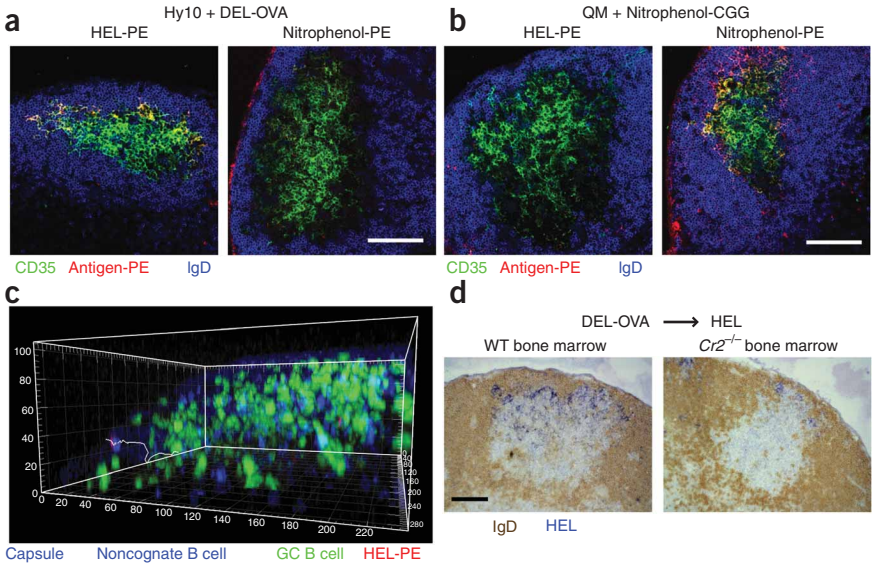

Figure 5 Noncognate B cells relay antigen opsonized by newly formed antibodies into the GC. (**a**) Hy10 B cells were adoptively transferred together with OT-II T cells and mice immunized with DEL-OVA. Mice were rechallenged 7 d later with either cognate HEL-PE (red, left panel) or noncognate nitrophenol-PE (red, right panel). Lymph nodes were stained for CD35 and IgD 8 h after challenge. (**b**) QM B cells were transferred and recipients challenged with nitrophenol-CGG. Mice were rechallenged 7 d later and analyzed as in **a**. Data in **a**,**b** are representative of three experiments. (**c**) Three-dimensional reconstruction of follicle in *Cr2*$^{-/-}$ bone marrow chimera imaged in **Supplementary Movie 2**, 7 d after DEL-OVA immunization. Capsule, blue; GC B cells, green; adoptively transferred WT follicular B cells, cyan; white track, movement of a CFP^{+}, HEL-PE immune complex–positive B cell. HEL-PE was injected 3 h before lymph node removal and imaging. (**d**) Immunohistochemical assessment of antigen distribution in WT and *Cr2*$^{-/-}$ bone marrow chimeras. Mice were challenged 7 d after immunization with HEL-OVA, and 8 h later draining lymph nodes were stained for HEL and IgD. Representative of three experiments. Scale bars in **a**,**b**,**d**, 100 μm; coordinates in **c**, distance in μm.

B cells (**Fig. 5d**). Thus follicular B cells deliver endogenously formed immune complexes into GCs in a CR1/2-dependent manner.

Immune complex relay drives antibody affinity maturation

Finally, we asked whether immune complex relay from SCS macrophages to B cells to the GC played any role in the GC response and affinity maturation. In initial experiments we noted that single-gene deficiencies in *Itgb2* (encoding the integrin β2 chain that is part of CR3), *Itgam* (encoding the α chain of CR3) or *Fcgr2b* (encoding FcγRIIb) had limited effects on the immune complex relay, suggesting redundant mechanisms of immune complex capture by SCS macrophages. These gene deficiencies therefore did not allow us to clearly assess the functional consequences of perturbations in the pathway. Moreover, attempts at genetic and pharmacological ablation of SCS macrophages either led to altered inflammatory conditions or affected other cell types, such as FDCs, that themselves affected the GC response (data not shown). We therefore turned to an alternative approach of testing the importance of the immune complex relay and examined the impact of disrupting the ability of noncognate B cells to function as antigen transport cells by removing complement receptors from these cells. Because CR1/2 also has a role on FDC and as a coreceptor on cognate B cells[19], we used the same adoptive transfer system as above, in which the FDC and cognate B cells were CR1/2 wild-type but the noncognate follicular B cells were either CR1/2-deficient or wild-type (**Supplementary Fig. 2** online). Thus, CR1/2-deficient or control bone marrow chimeras received adoptive transfer of small numbers of wild-type, antigen-specific Hy10 B cells and OT-II T cells and were then immunized with DEL-OVA in a depot-forming adjuvant, and the GC response mounted by the CR1/2-sufficient Hy10 B cells was examined. At day 7, before affinity maturation, the magnitude of the GC and antibody response was equivalent in the two groups, suggesting that cognate B cells were able to directly access antigen from SCS macrophages or other sources and initiate the response (**Supplementary Fig. 2**). However, at day 14 the magnitude of the GC response in mice lacking immune complex transport–competent B cells was approximately half that of mice reconstituted with wild-type B cells (**Fig. 6a**,**b**). Notably, whereas class switching occurred normally, there was less affinity maturation as assessed by flow cytometry for GC B cell binding of the low-affinity antigen (**Fig. 6a**,**b**) and serum antibody binding by ELISA (**Fig. 6c**). Thus, although serum anti-HEL Igκ titers were similarly increased from day 7 to day 14, there was a less marked rise in high affinity anti-DEL Igκ antibodies in *Cr2*$^{-/-}$ bone marrow chimera recipients than in wild-type chimeras (**Fig. 6c**). To directly show that there was a difference in affinity-based selection, we sorted single cells from recipient mice by flow cytometry on day 14 of the response and PCR-amplified and analyzed the *Igh* variable region gene for somatic hypermutation (**Fig. 6d**). Sequence analysis showed significantly more enrichment of Hy10 B cells with the canonical high-affinity Y53F mutation[11] in wild-type (34 of 46 sequences) than *Cr2*$^{-/-}$ bone marrow chimeras (23 of 53; $P = 0.002$, Fisher's exact test). Although disruption of immune complex relay affected the GC B cell response there was no significant difference in the number of OT-II T cells recovered (**Supplementary Fig. 2**). These data indicate that follicular B cells transport opsonized antigen into GC light zones to enhance the GC response and that affinity maturation is blunted when this immune complex relay pathway is disrupted.

DISCUSSION

The above findings demonstrate that SCS macrophages are a distinct, poorly endocytic macrophage cell type with low degradative capacity. These LT$\alpha_1\beta_2$-dependent cells deliver intact antigen-containing immune complexes captured in the SCS along membrane processes into the follicle. Newly generated immune complexes are delivered to the GC light zone in a CR1/2-dependent manner by antigen-transporting B cells, a process that influences the magnitude and quality of the GC response. Together these findings suggest that the relay of immune complexes from SCS macrophages to follicular B cells and then to light-zone FDCs and GC B cells helps drive antibody affinity maturation by mediating the ongoing GC delivery of antigen and competing antibody.

Early electron microscopy studies of horseradish peroxidase–containing immune complexes deposited on cells in the SCS floor suggested that they were sequestered on the cell surface or in plasma membrane infoldings[3]. More recently, electron microscopy of captured vesicular stomatitis virus showed virions on the cell surface but also in vacuoles[6]. Two-photon microscopy revealed that B cells could capture antigens and immune complexes from SCS macrophages, further

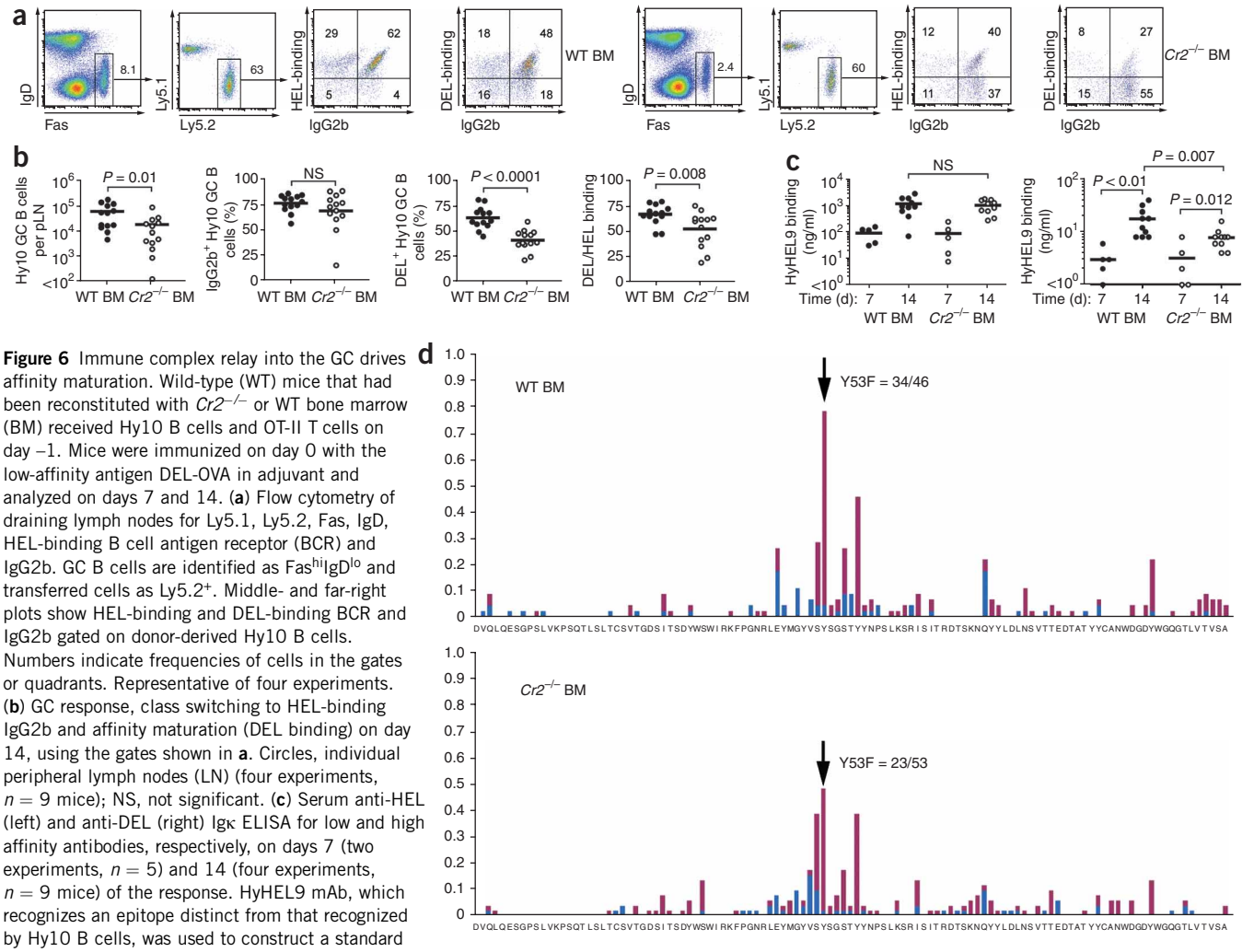

Figure 6 Immune complex relay into the GC drives affinity maturation. Wild-type (WT) mice that had been reconstituted with $Cr2^{-/-}$ or WT bone marrow (BM) received Hy10 B cells and OT-II T cells on day –1. Mice were immunized on day 0 with the low-affinity antigen DEL-OVA in adjuvant and analyzed on days 7 and 14. (**a**) Flow cytometry of draining lymph nodes for Ly5.1, Ly5.2, Fas, IgD, HEL-binding B cell antigen receptor (BCR) and IgG2b. GC B cells are identified as $Fas^{hi}IgD^{lo}$ and transferred cells as $Ly5.2^{+}$. Middle- and far-right plots show HEL-binding and DEL-binding BCR and IgG2b gated on donor-derived Hy10 B cells. Numbers indicate frequencies of cells in the gates or quadrants. Representative of four experiments. (**b**) GC response, class switching to HEL-binding IgG2b and affinity maturation (DEL binding) on day 14, using the gates shown in **a**. Circles, individual peripheral lymph nodes (LN) (four experiments, $n = 9$ mice); NS, not significant. (**c**) Serum anti-HEL (left) and anti-DEL (right) Igκ ELISA for low and high affinity antibodies, respectively, on days 7 (two experiments, $n = 5$) and 14 (four experiments, $n = 9$ mice) of the response. HyHEL9 mAb, which recognizes an epitope distinct from that recognized by Hy10 B cells, was used to construct a standard curve for quantification of antibody. (**d**) Somatic hypermutation at day 14. Mice were immunized as above and donor-derived GC B cells sorted on day 14 for single-cell PCR and sequence analysis. Arrow, Tyr53 position. Replacement mutations, red; silent mutations, blue. Frequency of Y53F mutations is significantly higher for WT (34/46) than $Cr2^{-/-}$ BM chimera recipients (23/53, $P = 0.002$, Fisher's exact test). Sequence data are from one sorting experiment.

establishing that these cells are able to display antigens on their cell surface[4–6]. Our analysis here of isolated cells demonstrated that SCS macrophages retained a greater proportion of the immune complexes they captured on their surface than the nearby medullary macrophages. Moreover, our data showed that these cells had less lysosomal function, a property that may facilitate recycling of internalized antigen back to the cell surface. As well as being necessary for their antigen presentation function, the lower degradative capacity of SCS macrophages might make them a 'safe haven' for some intracellular pathogens[20].

Ultrastructural studies and intravital two-photon microscopy have shown that macrophage processes ('heads') protrude into the SCS and are positioned in the lymph flow to capture immune complexes as they drain from the afferent lymphatic vessel[2–6,21]. By tracking the behavior of captured complexes on SCS macrophage 'tail' processes, we found that immune complexes fragmented as they were moved along the process—perhaps an effect of forces exerted on the complexes as they passed the junction between the SCS macrophage and the sinus lining cells they insert themselves through[3]. The basis for the unidirectional movement of particles along the macrophage surface is not yet clear, but in preliminary analysis we found that the macrophages had a polarized distribution of transmembrane proteins (T.G.P., E.E.G. and J.G.C., unpublished data), suggesting that they are organized to mediate directional membrane transport. Anterograde membrane flow is a common feature of polarized migrating cells and is sufficient to move a variety of particle types over the membrane surface in an actin-dependent manner[22]. T cells polarizing toward a target cell show directed movement of membrane over their surface to the site of synapse[23,24]. It seems possible that a related form of surface molecule treadmilling could occur to promote unidirectional movement of immune complex binding proteins in SCS macrophages. Alternatively, perhaps there is sufficient lymph flow over the surface of SCS macrophages to provide shear forces that mediate directional movement of surface molecules. Shear forces exerted by hydrodynamic flow cause 'sailing' of immune complexes on the trypanosome membrane surface[25]. Finally, the possibility that immune complexes are transported inside the cell in a specialized form of transcytosis is not yet excluded. Future studies will need to characterize the membrane polarity of SCS macrophages and determine the molecular requirements for SCS-to-follicule movement of immune complexes.

B cell–derived $LT\alpha_1\beta_2$ has an established role in promoting FDC development in lymphoid tissues[14]. $LT\alpha_1\beta_2$ is also required for maintenance of marginal zone macrophage populations in the spleen[14] and for homeostasis of splenic dendritic cells[26]. The dependence of lymph node SCS macrophages on $LT\alpha_1\beta_2$ suggests that disruption in antigen

relay, as well as the loss of FDCs, contributes to the impaired antibody responses observed in LTα-deficient mice[14,15]. The impact of depleting these cells should be considered during the ongoing clinical trials of $LT\alpha_1\beta_2$ antagonism in humans[15]. The role of B cells as a key source of $LT\alpha_1\beta_2$ for SCS macrophage development or maintenance indicates that B cell follicles help themselves acquire a uniform coverage of SCS macrophages. This interplay is likely to ensure that as a lymph node enlarges in response to immunization or infection and the B cell representation increases because of recruitment, retention and proliferation, the overlying SCS macrophage population increases concordantly.

The demonstration that CR1/2 on noncognate follicular B cells is important for immune complex delivery to the GC establishes a third site where CR1/2 acts during the antibody response, a finding that may resolve some of the discrepancies in earlier investigations examining the role of CR1/2 on FDCs or cognate B cells[19]. The importance of follicular B cells in mediating antigen delivery to the GC is consistent with the recent demonstration that follicular B cells gain access to the GC light zone[10,11]. As well as delivering immune complexes to FDCs, immune complex–laden follicular B cells seem likely to play a direct role in presentation as they travel through the GC. Antigen encounter by B–B cellular interactions might help explain how, in some studies, GC formation and somatic hypermutation could take place in the apparent absence of immune complex–capturing FDCs[27,28]. Although it has long been suggested that the early antibody response is important in the later GC response, this has largely been studied by testing the effects of exogenously administered antibody on the endogenous response[29–31]. An exception is the finding that mice with targeted disruption of the IgM secretory region, which lack secreted IgM, have an impaired GC response and delayed affinity maturation[32,33]. Whether this reflected a role of natural antibody or newly produced antibody was unclear. The macrophage–B cell immune complex relay that we describe may principally have arisen to mediate efficient delivery of even minute amounts of antigen, as well as antibody, to the GC to help drive ongoing affinity maturation. Approaches to target antigens to SCS macrophages and that thus facilitate delivery to GCs might allow improved vaccine design.

METHODS

Methods and any associated references are available in the online version of the paper at http://www.nature.com/natureimmunology/.

Accession codes. UCSD-Nature Signaling Gateway (http://www.signaling-gateway.org): A000541. GEO: microarray data, GSE15767.

Note: Supplementary information is available on the Nature Immunology website.

ACKNOWLEDGMENTS

We thank L. Shiow for cell sorting and discussions, K. Suzuki for preparation of HEL-PE, C. Allen for help with single cell sorting, I. Girgorova for help with video editing, J. An for mouse screening, J. Atkinson (Washington University) for CR2-deficient mice, M. Wabl (University of California, San Francisco) for QM mice, J. Browning (Biogen Idec) for LTβR-Fc, P. Crocker (University of Glasgow) for Ser-4 antibody, A. Bullen and M. Krummel for help with the two-photon microscope, A. Bankovich for advice, the UCSF Hybridoma Core, the Gladstone Genomics Core and the Diabetes and Endocrinology Research Center Microscopy Core and Biological Imaging Development Center. Supported by an Australian National Health and Medical Research Council CJ Martin fellowship (T.G.P.), a US National Science Foundation graduate research fellowship (J.A.G.), a Howard Hughes Medical Institute investigator award (J.G.C.), the US National Institutes of Health (AI45073 and AI40098) and a Sandler New Technology Award.

AUTHOR CONTRIBUTIONS

T.G.P. and J.G.C. designed and conceptualized the research; T.G.P., J.A.G. and E.E.G. did the experiments; Y.X. performed the microarray and Q-PCR analysis; T.G.P., J.A.G., E.E.G. and J.G.C. analyzed the data; T.G.P., J.A.G. and E.E.G. prepared figures; T.G.P. and J.G.C. wrote the manuscript.

Published online at http://www.nature.com/natureimmunology/
Reprints and permissions information is available online at http://npg.nature.com/reprintsandpermissions/

1. Nossal, G.J., Abbot, A., Mitchell, J. & Lummus, Z. Antigens in immunity. XV. Ultrastructural features of antigen capture in primary and secondary lymphoid follicles. *J. Exp. Med.* **127**, 277–290 (1968).
2. Fossum, S. The architecture of rat lymph nodes. IV. Distribution of ferritin and colloidal carbon in the draining lymph nodes after foot-pad injection. *Scand. J. Immunol.* **12**, 433–441 (1980).
3. Szakal, A.K., Holmes, K.L. & Tew, J.G. Transport of immune complexes from the subcapsular sinus to lymph node follicles on the surface of nonphagocytic cells, including cells with dendritic morphology. *J. Immunol.* **131**, 1714–1727 (1983).
4. Carrasco, Y.R. & Batista, F.D. B cells acquire particulate antigen in a macrophage-rich area at the boundary between the follicle and the subcapsular sinus of the lymph node. *Immunity* **27**, 160–171 (2007).
5. Phan, T.G., Grigorova, I., Okada, T. & Cyster, J.G. Subcapsular encounter and complement-dependent transport of immune complexes by lymph node B cells. *Nat. Immunol.* **8**, 992–1000 (2007).
6. Junt, T. *et al.* Subcapsular sinus macrophages in lymph nodes clear lymph-borne viruses and present them to antiviral B cells. *Nature* **450**, 110–114 (2007).
7. Steinman, R.M. & Banchereau, J. Taking dendritic cells into medicine. *Nature* **449**, 419–426 (2007).
8. MacLennan, I.C.M. Germinal centers. *Annu. Rev. Immunol.* **12**, 117–139 (1994).
9. Allen, C.D., Okada, T. & Cyster, J.G. Germinal-center organization and cellular dynamics. *Immunity* **27**, 190–202 (2007).
10. Schwickert, T.A. *et al. In vivo* imaging of germinal centres reveals a dynamic open structure. *Nature* **446**, 83–87 (2007).
11. Allen, C.D., Okada, T., Tang, H.L. & Cyster, J.G. Imaging of germinal center selection events during affinity maturation. *Science* **315**, 528–531 (2007).
12. Crocker, P.R. & Gordon, S. Properties and distribution of a lectin-like hemagglutinin differentially expressed by murine stromal tissue macrophages. *J. Exp. Med.* **164**, 1862–1875 (1986).
13. Hume, D.A., Robinson, A.P., MacPherson, G.G. & Gordon, S. The mononuclear phagocyte system of the mouse defined by immunohistochemical localization of antigen F4/80. Relationship between macrophages, Langerhans cells, reticular cells, and dendritic cells in lymphoid and hematopoietic organs. *J. Exp. Med.* **158**, 1522–1536 (1983).
14. Fu, Y.-X. & Chaplin, D.D. Development and maturation of secondary lymphoid tissues. *Annu. Rev. Immunol.* **17**, 399–433 (1999).
15. Browning, J.L. Inhibition of the lymphotoxin pathway as a therapy for autoimmune disease. *Immunol. Rev.* **223**, 202–220 (2008).
16. Ngo, V.N., Cornall, R.J. & Cyster, J.G. Splenic T zone development is B cell dependent. *J. Exp. Med.* **194**, 1649–1660 (2001).
17. Cascalho, M., Ma, A., Lee, S., Masat, L. & Wabl, M. A quasi-monoclonal mouse. *Science* **272**, 1649–1652 (1996).
18. Germain, R.N., Miller, M.J., Dustin, M.L. & Nussenzweig, M.C. Dynamic imaging of the immune system: progress, pitfalls and promise. *Nat. Rev. Immunol.* **6**, 497–507 (2006).
19. Roozendaal, R. & Carroll, M.C. Complement receptors CD21 and CD35 in humoral immunity. *Immunol. Rev.* **219**, 157–166 (2007).
20. Chtanova, T. *et al.* Dynamics of neutrophil migration in lymph nodes during infection. *Immunity* **29**, 487–496 (2008).
21. Farr, A.G., Cho, Y. & De Bruyn, P.P. The structure of the sinus wall of the lymph node relative to its endocytic properties and transmural cell passage. *Am. J. Anat.* **157**, 265–284 (1980).
22. Prigozhina, N.L. & Waterman-Storer, C.M. Protein kinase D-mediated anterograde membrane trafficking is required for fibroblast motility. *Curr. Biol.* **14**, 88–98 (2004).
23. Wulfing, C. & Davis, M.M. A receptor/cytoskeletal movement triggered by costimulation during T cell activation. *Science* **282**, 2266–2269 (1998).
24. Moss, W.C., Irvine, D.J., Davis, M.M. & Krummel, M.F. Quantifying signaling-induced reorientation of T cell receptors during immunological synapse formation. *Proc. Natl. Acad. Sci. USA* **99**, 15024–15029 (2002).
25. Engstler, M. *et al.* Hydrodynamic flow-mediated protein sorting on the cell surface of trypanosomes. *Cell* **131**, 505–515 (2007).
26. Kabashima, K. *et al.* Intrinsic lymphotoxin-beta receptor requirement for homeostasis of lymphoid tissue dendritic cells. *Immunity* **22**, 439–450 (2005).
27. Wang, Y. *et al.* Antigen persistence is required for somatic mutation and affinity maturation of immunoglobulin. *Eur. J. Immunol.* **30**, 2226–2234 (2000).
28. Hannum, L.G., Haberman, A.M., Anderson, S.M. & Shlomchik, M.J. Germinal center initiation, variable gene region hypermutation, and mutant B cell selection without detectable immune complexes on follicular dendritic cells. *J. Exp. Med.* **192**, 931–942 (2000).
29. Brady, L.J. Antibody-mediated immunomodulation: a strategy to improve host responses against microbial antigens. *Infect. Immun.* **73**, 671–678 (2005).
30. Getahun, A. & Heyman, B. How antibodies act as natural adjuvants. *Immunol. Lett.* **104**, 38–45 (2006).
31. Song, H., Nie, X., Basu, S. & Cerny, J. Antibody feedback and somatic mutation in B cells: regulation of mutation by immune complexes with IgG antibody. *Immunol. Rev.* **162**, 211–218 (1998).
32. Ehrenstein, M.R., O'Keefe, T.L., Davies, S.L. & Neuberger, M.S. Targeted gene disruption reveals a role for natural secretory IgM in the maturation of the primary immune response. *Proc. Natl. Acad. Sci. USA* **95**, 10089–10093 (1998).
33. Boes, M. *et al.* Enhanced B-1 cell development, but impaired IgG antibody responses in mice deficient in secreted IgM. *J. Immunol.* **160**, 4776–4787 (1998).

ONLINE METHODS

Mice. Wild-type and Ly5.2 (CD45.1) congenic mice C57BL/6 (B6), 6–12 weeks old, were from either National Cancer Institute or Jackson Laboratories. B6 mice expressing CFP under the β-actin promoter[34] (004218; Tg(ACTB-ECFP)1Nagy/J), mice expressing GFP under the human ubiquitin promoter[35] (004353; Tg(UBC-GFP)30Scha/J) and B cell–deficient *Igh-6*$^{-/-}$ mice[36] (002288; B6.129S2-*Igh-6*^{tm1Cgn}/J), were from Jackson Laboratories. Mice deficient for LTα[37] (B6.129S2-*Lta*^{tm1DCh}) and LTβR[38] and mice overexpressing membrane-bound LTα under the Igκ promoter (line b10) have been described[16] and were ten or more generations backcrossed to B6. Homozygous 6-month-old κLTα transgenic mice and age-matched controls were analyzed. *Cr2*$^{-/-}$ mice deficient for both CR1 and CR2 (ref. 39), Hy10 mice (previously named VDJ9/κ5 mice) expressing a knock-in BCR with high affinity for hen egg lysosome (HEL) and low affinity for duck egg lysozyme (DEL)[11] and OT-II TCR transgenic mice[40] were all ten or more generations backcrossed to B6. Hy10 mice homozygous for the ubiquitin-GFP transgene were used for imaging studies. QM mice expressing knock-in BCR specific for nitrophenol were as described[17]. Animals were housed in a specific pathogen–free environment in the Laboratory Animal Research Center at UCSF and all experiments conformed to the ethical principles and guidelines approved by the UCSF Institutional and Animal Care and Use Committee.

Bone marrow chimeras and adoptive transfers. Ly5.2 congenic mice were lethally irradiated with either 1,100 or 1,300 rad in split doses and reconstituted with 1–3 × 10^6 bone marrow cells from wild-type and *Cr2*$^{-/-}$ donors. Mixed bone marrow chimeras were made with a 80:20 mix of *Ltbr*$^{-/-}$:Ly5.2 bone marrow into wild-type (Ly5.1) recipients. Mice were analyzed 8–12 weeks later. For B cell reconstitution experiments, B cells were negatively isolated from wild-type or *Lta*$^{-/-}$ mice using the AutoMACS magnetically activated cell separator (Miltenyi) and biotinylated antibodies to CD11c (clone HL3) and CD43 (clone S7) (both from BD Pharmingen) and MACS streptavidin microbeads (Miltenyi) as described[5]. We transferred 2–3 × 10^7 B cells into *Igh-6*$^{-/-}$ mice and analyzed recipient mice 14 d later. B cells were typically >95% pure as assessed by flow cytometric analysis on a FACSCalibur (BD Biosciences). Transferred B cells typically constituted 2%–8% of lymph node cells.

***In vivo* immune complex generation and endocytosis.** PE immune complexes were generated as described[5]. To generate BSA–anti-BSA immune complexes, polyclonal rabbit IgG antibodies to BSA (Invitrogen) were dialyzed and conjugated to Alexa Fluor 647 (Molecular Probes). Mice were given 2 mg intraperitoneally of the labeled antibody 12–16 h before subcutaneous (s.c.) injection of 20 μg of DQ Green–BSA (Invitrogen) per draining lymph node. For analysis, cells were isolated from draining lymph nodes together with lymph nodes from a Ly5.2 congenic mouse that did not receive immune complexes, as described[5].

Tissue digestion and flow cytometry. Lymph nodes were carefully dissected free of fat and fasciae and gently teased apart with microforceps into DMEM containing penicillin, streptomycin and HEPES buffer, pH 7.2. The tissue was then digested with Liberase Blendzyme 2 (Roche Applied Science) at 0.2 mg/ml and DNase I at 20 μg/ml for 20–30 min. Proteases were then inactivated with 10% FBS and 5 μM EDTA (unless immune complexes were present) and disaggregated by passing through a 100-μm nylon sieve (BD Bioscience). Single cells were then washed, blocked with 2.4G2 (UCSF Hybridoma Core Facility) to block FcgRIIb and FcgRIII, as well as with 5% normal mouse and normal rat serum, and stained for flow cytometric analysis as described[5]. For identifying SCS macrophages, Ser-4 mAbs to CD169 (ref. 41) were purified from ascites fluid and conjugated to either Alexa Fluor 488 or Alexa Fluor 647 using the antibody labeling kits from Molecular Probes. Antibodies used included PE- and PerCp-conjugated anti-B220 (clone RA3-6B2, BD Pharmingen), PerCp-conjugated anti-CD4 (clone RM4-5, BD Pharmingen), PerCp-conjugated anti-CD8α (clone 53-6.7, BD Pharmingen), FITC- or PE-conjugated CD11b (clone Mac-1, Invitrogen), FITC- or PE-conjugated CD11c (clone HL3, BD Pharmingen), Pacific Blue–conjugated anti-CD45.1 (clone A20, Biolegend), Alexa Fluor 700– or Pacific Blue–conjugated anti-CD45.2 (clone 104, Biolegend), biotin-conjugated anti-F4/80 (clone C1:A3-1, Cedarlane), Alexa Fluor 647–conjugated anti-F4/80 (clone Cl:A3-1, Biolegend) and Qdot 605–conjugated streptavidin (Molecular Probes). DEL was purified as described[11]. For analysis of B cell responses, HEL (Sigma) and DEL were directly conjugated to Alexa Fluor 647 and conjugated antigen isolated using Bio-Spin 6 columns (Bio-Rad). GC cells were identified with antibodies to FITC-conjugated anti-IgD (clone 11-26c.2a, BD Pharmingen), PE-conjugated anti-Fas (clone Jo2, BD Pharmingen), and biotin-conjugated anti-IgG2b (clone RMG2b-1, Biolegend). HEL–Alexa Fluor 647 was used to detect HEL-specific B cells and DEL–Alexa Fluor 647 used to detect somatically mutated cells that had acquired high affinity for the original antigen[11]. Plasma cells were identified by intracellular staining as described[42]. Briefly, cells were fixed for 20 min in 2% paraformaldehyde and then permeabilized overnight with 0.2% polyethylene sorbitan monolaurate before washing and staining with HEL–Alexa Fluor 647 and biotin-conjugated anti-syndecan-1 (clone 281-2, BD Pharmingen), PE-conjugated anti-B220 and FITC-conjugated anti-CD45.1 (BD Pharmingen). Intracellular staining for LAMP-1 and LAMP-2 was performed with FITC-conjugated anti-LAMP-1 (clone 1D4B, BD Pharmingen) and anti-LAMP-2 (clone ABL-93, BD Pharmingen), respectively. Staining for surface expression of LTβR was performed using purified hamster mAb AF:H6 and detected with anti-Armenian and Syrian hamster IgG cocktail conjugated to PE (BD Pharmingen) as described[26]. Data were acquired on an LSRII (BD Biosciences) and analyzed using FlowJo software (Treestar).

Stripping of surface-bound immune complexes. In acid stripping experiments, mice were administered PE immune complexes and 4 h later lymph node cells were washed in PBS at 4 °C before exposure to 0.5 M NaCl, 0.2 M acetic acid for 4 min at 4 °C (ref. 43). Cells were then washed three times before staining.

Macrophage isolation and cell sorting. For cell sorting, lymph node cells prepared as above were resuspended in DMEM, 2% FBS, 5 μM EDTA and loaded onto an ice-cold density gradient layered with 50% and 30% Percoll (Amersham). The column was spun at 365*g* for 25 min with no braking. The 50%/30% interface contained large cells that were typically enriched tenfold for CD169-expressing cells. Fc receptors were then blocked with 2.4G2 in 5% normal rat serum and 5% normal mouse serum before staining in DMEM, 2% FBS, 5 μM EDTA with anti-CD11c–FITC, anti-CD11b–PE, anti-B220–PerCp, anti-CD4–PerCp, anti-CD8–PerCp, anti-CD169–Alexa Fluor 647, anti-F4/80–biotin and streptavidin–Qdot 605. Live single cells that excluded DAPI (Molecular Probes) were gated and sorted for CD11c^{int}CD11b^{+}B220^{-}CD4^{-}CD8^{-}CD169^{hi}F4/80^{-} (SCS macrophage) and CD11c^{int}CD11b^{+}B220^{-}CD4^{-}CD8^{-}CD169^{hi}F4/80^{+} (medullary macrophage) subsets on a FACSAria (BD Biosciences). Cells were typically ~95% pure when reanalyzed for cell sorting parameters.

Gene expression profiling and real-time PCR. Total RNA was isolated from ~20,000 sorted SCS and medullary macrophages with the RNEasy Micro Kit (Qiagen). RNA was amplified using the Ovation RNA Amplification System V2 and amplified cDNA fragmented and labeled with FL-Ovation cDNA Biotin Module V2 (both from NuGen). Samples from three independent experiments were then hybridized to Affymetrix Genechip array, stained, scanned and normalized by the UCSF Gladstone Genomics Core facility. Normalized data were analyzed using Remote Analysis Computation for gene Expression data (http://race.unil.ch/). Housekeeping genes used to validate the microarray were from ref. 44. The list of macrophage transcription factors used to establish the hematopoietic cell lineage of sorted cells was from ref. 45. Gene expression profiles in **Figure 3b,c,e** were defined as those with probe signals >2^6 and a Bayesian false discovery rate <0.05. For Q-PCR, unamplified cDNA was reacted with primer–probe sets (Integrated DNA Technologies) and SYBR Green PCR Master Mix (Applied Biosystems) on a 7300 Real-Time PCR System (Applied Biosystems). The relative mRNA abundance of target genes was determined by subtracting the threshold cycle for the housekeeping gene (*Hprt1*) from the target gene.

Adoptive transfers and immunizations. T-dependent immune response was tracked using Hy10 B cells as described[11]. Briefly, IgM^{a}-expressing HEL-specific B cells were negatively isolated from Hy10 mice by AutoMACS, depleting cells labeled with biotinylated antibodies to CD11c, CD43, Ly6C (clone AL-21, BD Pharmingen), IgM^{b} (clone AF6-78) and IgD^{b} (clone 217-170; both from

doi:10.1038/ni.1745

BD Pharmingen), plus MACS streptavidin microbeads. Frequency of HEL-specific B cells was typically ~70%, as assessed by flow cytometric staining for IgM^a (clone DS-1, BD Pharmingen) and HEL binding. OVA-specific T cells were negatively isolated from OT-II mice by AutoMACS, depleting cells labeled with biotinylated antibodies to B220 (clone RA3-6B2, BD Pharmingen), CD11b (clone Mac-1, CALTAG), CD11c and Ly6C (clone AL-21) plus MACS streptavidin microbeads. Frequency of OVA-specific T cells was typically ~70% as assessed by flow cytometry for V_α2-FITC (clone B20.1) and V_β5-PE (clone MR9-4; both from BD Pharmingen). We then adoptively transferred 10^5 HEL-specific B cells and OVA-specific T cells into wild-type or *Cr2*$^{-/-}$ bone marrow chimeras. Mice were then challenged with 10 μg of DEL-OVA in Sigma Adjuvant System (Sigma) in both lateral chest walls below the scapula (to drain to the brachial lymph nodes) and both flanks and 5 μg in both tail base (to drain to the inguinal lymph nodes). Seven or 14 d later, serum was collected for ELISA and lymph nodes removed for flow cytometry and histology. For assessment of antigen transport into the GC, Hy10 B cells and OT-II T cells were adoptively transferred into Ly5.1 congenic recipients, and the recipients were immunized with DEL-OVA as above. On day 7, mice were given additional specific antigen HEL-PE or nonspecific nitrophenol-PE. Draining lymph nodes were collected 8 h later for immunofluorescence microscopy. Reciprocally, QM B cells specific for nitrophenol were adoptively transferred and mice immunized with nitrophenol-CGG. On day 7 mice were rechallenged with either HEL-PE or nitrophenol-PE and analyzed for deposition of opsonized antigen in GCs 8 h later. To test the requirements for B cell antigen transport, wild-type or *Cr2*$^{-/-}$ bone marrow chimeric recipients were rechallenged on day 7 with HEL-OVA and lymph nodes collected 8 h later for immunohistochemistry. For two-photon microscopy, 9.5×10^4 Hy10 B cells and 5×10^3 Hy10 B cells expressing GFP were transferred together with 10^5 OT-II T cells and mice challenged with DEL-OVA in adjuvant. On day 7, mice were rechallenged s.c. with 10 μg HEL-PE and 3–4 h later draining lymph nodes collected. HEL-PE was produced by incubating HEL-biotin in molar excess with streptavidin-PE and removing unbound HEL-biotin using the Bio-Spin 30 column (Bio-Rad).

ELISA. ELISA was performed as described[46]. Briefly, 96-well polystyrene plates (Nunc) were coated with 10 μg/ml of either HEL or DEL at 4 °C overnight and then blocked with 5% skim milk powder in PBS. Sera in 0.1% BSA in PBS were then serially diluted in duplicate together with HyHEL9 and HyHEL10 mAbs[47] (grown in-house) as positive control for anti-HEL ELISA. For anti-DEL ELISA, the HyHEL10 mAb (which has the same specificity as the Hy10 knock-in BCR) did not react with DEL and served as a negative control, and HyHEL9 mAb, which recognized a different epitope[48], served as a positive control. Bound antibodies were detected with biotinylated anti-Igκ clone 187.1 (BD Pharmingen) in 0.1% BSA, 1% skim milk in PBS. Streptavidin–alkaline phosphatase (AP) (Jackson Immunoresearch) was visualized with the substrate *p*-nitrophenyl phosphate (Fisher) and the absorbance read at 405 nm on a SpectraMax spectrophotometer (Molecular Devices). A standard curve was constructed for the HyHEL9 mAb and used to determine the equivalent amounts of HEL- and DEL-specific Igκ antibodies.

Light and fluorescence microscopy. Sorted SCS and medullary macrophages were resuspended at 10^7 cells/ml in 10% FBS in RPMI and incubated on glass coverslips (Fisher) at 37 °C for >4 h. Adherent cells were fixed for 20 min with 2% paraformaldehyde and then permeabilized with 0.05% Triton X-100 before washing and restaining with anti-CD169–Alexa Fluor 647, anti-LAMP-1–PE (clone 1D4B, BD Pharmingen) and DAPI. The coverslip was then mounted on a glass slide with Fluoromount-G (Southern Biotechnology) and DIC and fluorescence images obtained with a Zeiss AxioObserver Z1 inverted microscope.

Immunohistochemistry was performed as described[11]. Briefly, 7-μm-thick lymph node sections were fixed in acetone and rehydrated with 0.1% BSA in Tris-buffered saline and blocked with 2% normal mouse serum, 0.1% BSA in Tris-buffered saline. Slides were washed and stained with anti-CD169 mAb detected with horseradish peroxidase–conjugated donkey anti–rat IgG (H+L) (Jackson Immunoresearch) blocked with 5% normal rat serum and stained with anti-B220–biotin detected with streptavidin-AP. HEL-binding plasma cells were identified by staining sections with HEL at 200 ng/ml followed by rabbit polyclonal IgG anti-HEL-biotin (Rockland) and detected with streptavidin-AP. GCs were identified as IgD-negative areas within the follicle by staining with anti-IgD-FITC detection with horseradish peroxidase–conjugated anti-FITC–(Roche Applied Science).

Immunofluorescence microscopy was performed as described[5]. Acetone-fixed 5-μm sections were stained with anti-CD169–Alexa Fluor 488, anti-F4/80-biotin and streptavidin-PE and allophycocyanin-conjugated anti-B220 (clone RA3-6B2, BD Pharmingen). Tiled images were captured and assembled on a Zeiss AxioObserver Z1. For confocal microscopy, 10–30-μm sections were stained with Ser-4–Alexa Fluor 488, anti-F4/80–biotin and streptavidin-PE (BD Pharmingen), and allophycocyanin-conjugated anti-B220 (clone RA3-6B2, BD Pharmingen) and images captured on a Leica TCS SL confocal microscope using the 488-, 543- and 633-nm laser lines to excite Alexa Fluor 488, PE and Alexa Fluor 647, respectively. Emission slits were tuned to 498–540 nm for FITC, 560–600 nm for PE and 643–710 nm for Alexa Fluor 647. Confocal images were processed using Adobe PhotoShop CS2.

Intravital microscopy and two-photon imaging. Intravital microscopy was performed essentially as described[5]. Mice were injected s.c. in the left flank and tail base with 20 μg of anti-CD169–Alexa Fluor 488 to label the SCS macrophages *in vivo* 12–16 h before imaging. For anesthesia, mice were injected with 500 μl intraperitoneally of anesthetic solution (ketamine 5 mg/ml and xylazine 1 mg/ml) and deep anesthesia maintained with 100–200 μl injected every 20–30 min as needed into the tail base contralateral to the imaging side. Anesthetized mice were given supplementary oxygen through a nose cone and positioned on a Biotherm Micro S37 stage warmer maintained at 37 °C. To image the inguinal lymph node, a skin flap was mobilized by blunt dissection and glued to a silicone base with Vetbond (3M). A window was made in the overlying skin and fat, connective tissue and fascia were carefully microdissected to reveal the cortical surface of the node. The node was then perfused with warm RPMI diffused with 5% CO_2:95% O_2 and imaged through the intact capsule. The temperature inside the meniscus was monitored and maintained at 35.8–37.5 °C with a single inline solution heater coupled to a temperature controller (Warner Instruments). To image the GC, HEL-specific Hy10 B cells expressing GFP were transferred into *Cr2*$^{-/-}$ bone marrow chimeras and challenged with DEL-OVA in adjuvant as above. The day before imaging, $1–3 \times 10^7$ CFP-expressing B cells were transferred to delineate the follicular mantle zone. On day 7, mice were rechallenged s.c. with 10 μg HEL-PE, and 3–4 h later draining lymph nodes were collected and explanted lymph nodes prepared for two-photon imaging as described[49]. Deep tissue images were acquired with a custom-built two-photon microscope (M. Krummel, UCSF). A MaiTai TiSapphire laser (Spectra-Physics) was tuned to provide an excitation wavelength of 910 nm. Each *xy* plane spanned 480 × 400 pixels at a 0.6 μm per pixel resolution, and 40–50 *xy* planes with 2–3 μm *z* spacings were formed by averaging 10 video frames every 20–30 s. Emission wavelengths used were 440–500 nm (CFP and second harmonic emission of collagen fibers), 500–550 nm (GFP and Alexa Fluor 488) and 567–640 nm (PE immune complexes and HEL-PE immune complexes). Images were acquired with Video Savant (IO Industries) and maximum intensity time-lapse images generated with MetaMorph (Molecular Devices). Videos were processed with a median noise filter. Cell tracks and three-dimensional rotation images were made with Imaris 5.01 × 64 (Bitplane) and images filtered with a median filter. Annotation and final movie compilation was performed in Adobe After Effects 7.0. Video files were converted to mpeg format with Avi to Mpeg Converter for Windows 1.5 (FlyDragon Software).

Single-cell PCR and somatic hypermutation analysis. For analysis of mutated sequences, single donor-derived GC B cells specific for HEL on day 14 of the response were sorted into 96-well plates and their *Igh* variable genes sequenced as described[11].

Statistical analysis. All statistical analysis was performed in Prism (GraphPad Software). Means between two groups were compared using one-tailed *t*-test. For analysis of somatic hypermutation data in **Figure 6d** we constructed a 2 × 2 contingency table and performed a Fisher's exact test.

34. Hadjantonakis, A.K., Macmaster, S. & Nagy, A. Embryonic stem cells and mice expressing different GFP variants for multiple non-invasive reporter usage within a single animal. *BMC Biotechnol.* **2**, 11 (2002).
35. Schaefer, B.C., Schaefer, M.L., Kappler, J.W., Marrack, P. & Kedl, R.M. Observation of antigen-dependent CD8+ T-cell/ dendritic cell interactions in vivo. *Cell. Immunol.* **214**, 110–122 (2001).
36. Kitamura, D., Roes, J., Kuhn, R. & Rajewsky, K. A B cell-deficient mouse by targeted disruption of the membrane exon of the immunoglobulin μ chain gene. *Nature* **350**, 423–426 (1991).
37. De Togni, P. *et al.* Abnormal development of peripheral lymphoid organs in mice deficient in lymphotoxin. *Science* **264**, 703–707 (1994).
38. Futterer, A., Mink, K., Luz, A., Kosco-Vilbois, M.H. & Pfeffer, K. The lymphotoxin beta receptor controls organogenesis and affinity maturation in peripheral lymphoid tissues. *Immunity* **9**, 59–70 (1998).
39. Molina, H. *et al.* Markedly impaired humoral immune response in mice deficient in complement receptors 1 and 2. *Proc. Natl. Acad. Sci. USA* **93**, 3357–3361 (1996).
40. Barnden, M.J., Allison, J., Heath, W.R. & Carbone, F.R. Defective TCR expression in transgenic mice constructed using cDNA-based alpha- and beta-chain genes under the control of heterologous regulatory elements. *Immunol. Cell Biol.* **76**, 34–40 (1998).
41. Crocker, P.R. & Gordon, S. Mouse macrophage hemagglutinin (sheep erythrocyte receptor) with specificity for sialylated glycoconjugates characterized by a monoclonal antibody. *J. Exp. Med.* **169**, 1333–1346 (1989).
42. Paus, D. *et al.* Antigen recognition strength regulates the choice between extrafollicular plasma cell and germinal center B cell differentiation. *J. Exp. Med.* **203**, 1081–1091 (2006).
43. Carroll, R.C. *et al.* Dynamin-dependent endocytosis of ionotropic glutamate receptors. *Proc. Natl. Acad. Sci. USA* **96**, 14112–14117 (1999).
44. Vandesompele, J. *et al.* Accurate normalization of real-time quantitative RT-PCR data by geometric averaging of multiple internal control genes. *Genome Biol.* **3**, RESEARCH0034 (2002).
45. Valledor, A.F., Borras, F.E., Cullell-Young, M. & Celada, A. Transcription factors that regulate monocyte/macrophage differentiation. *J. Leukoc. Biol.* **63**, 405–417 (1998).
46. Phan, T.G. *et al.* B cell receptor-independent stimuli trigger immunoglobulin (Ig) class switch recombination and production of IgG autoantibodies by anergic self-reactive B cells. *J. Exp. Med.* **197**, 845–860 (2003).
47. Smith-Gill, S.J., Mainhart, C.R., Lavoie, T.B., Rudikoff, S. & Potter, M. VL-VH expression by monoclonal antibodies recognizing avian lysozyme. *J. Immunol.* **132**, 963–967 (1984).
48. Smith-Gill, S.J., Lavoie, T.B. & Mainhart, C.R. Antigenic regions defined by monoclonal antibodies correspond to structural domains of avian lysozyme. *J. Immunol.* **133**, 384–393 (1984).
49. Okada, T. *et al.* Antigen-engaged B cells undergo chemotaxis toward the T zone and form motile conjugates with helper T cells. *PLoS Biol.* **3**, e150 (2005).

doi:10.1038/ni.1745